Atomic Structure and Chemistry of High-Entropy Oxide Grain Boundaries revealed by STEM Imaging, Strain Mapping, and Spectroscopy

Huiming Guo, Hasti Vahidi, Hyojoo Kang, Soham Shah, Mingjie Xu, Toshihiro Aoki, Timothy J Rupert, Jian Luo, Kandis Leslie Gilliard-AbdulAziz, William J Bowman







Microscopy

Microanalysis

Atomic Structure and Chemistry of High-Entropy Oxide Grain Boundaries revealed by STEM Imaging, Strain Mapping, and Spectroscopy

Huiming Guo¹, Hasti Vahidi¹, Hyojoo Kang^{1,2}, Soham Shah³, Mingjie Xu⁴, Toshihiro Aoki⁴, Timothy J. Rupert¹, Jian Luo⁵, Kandis Leslie Gilliard-AbdulAziz^{3,6}, and William J. Bowman^{1,4,*}

Compositionally complex oxides (CCOs) are an emerging class of materials encompassing high entropy oxides and entropy stabilized oxides (HEOs, ESOs) whose compositional complexity can be used to modify chemical bond structure, lattice distortion and ranges of disorder for advanced functional properties [1-5]. Grain boundary (GB) and point defect segregation to GBs is relatively understudied in CCOs even though they can govern macroscopic material properties [6, 7]. For example, GB segregation governs GB chemical order and disorder as well as point defect distribution, so it plays a critical role in GB electrochemical kinetics, which commonly serve as the rate-determined step of electrode reaction, charge transport and mass diffusion. However, compared with conventional oxides, GBs in multi-cation CCO systems are expected to exhibit more complex segregation phenomena and thus prove more difficult to tune through GB design strategies.

In this work, GB segregation study was done on a model perovskite CCO LaFe_{0.7}Ni_{0.1}Co_{0.1}Cu_{0.05}Pd_{0.05}O_{3-x} textured thin film with (sub-)atomic-resolution aberration-corrected scanning transmission electron microscopy (STEM) companied with energy spectroscopy analysis, such as energy dispersive X-ray spectroscopy (EDS) and electron energy-loss spectroscopy (EELS), and geometric phase analysis (GPA) to decipher the role of cation constituents and GB nanostructure in cation segregation concentration of CCO GBs[8]. It is found that GB segregation is correlated with cation reducibility which can be predicted by the Ellingham diagram, as Pd and Cu with high reducibility significantly segregate at GBs with oxygen deficiency, relative to other CCO constituents (Fig. 1A-J). Additionally, by tracking changes of the O-K edge EELS pre-peak, oxygen deficiency at GBs corresponds to accumulation of V_{0} , indicating that cation reducibility governs the demixing order of CCO GBs by determining cation cosegregation energy with $V_{\rm O}$ (Fig. 1K-L). Furthermore, the segregation of Pd and Cu tend upwards with the concentration and spatial distribution of V_O along the GB plane fluctuated by GB atomic structure and strong elastic strain induced by GB local disorder, such as dislocations (Fig. 2). This work offers a perspective of controlling segregation concentration of CCO GBs by tuning reducibility of CCO cations and oxygen deficiency, which is expected to guide GB design in CCOs for property improvement[9].

¹Department of Materials Science and Engineering, University of California Irvine, Irvine, CA, United States

²Department of Materials Science and Engineering, Yonsei University, Seoul, South Korea

³Department of Chemical and Environmental Engineering, University of California Riverside, Riverside, CA, United States

⁴Irvine Materials Research Institute (IMRI), University of California Irvine, Irvine, CA, United States

⁵Department of NanoEngineering, University of California San Diego, La Jolla, CA, United States

⁶Department of Civil and Environmental Engineering, University of Southern California, Los Angeles, CA, United States

^{*}Corresponding author: will.bowman@uci.edu

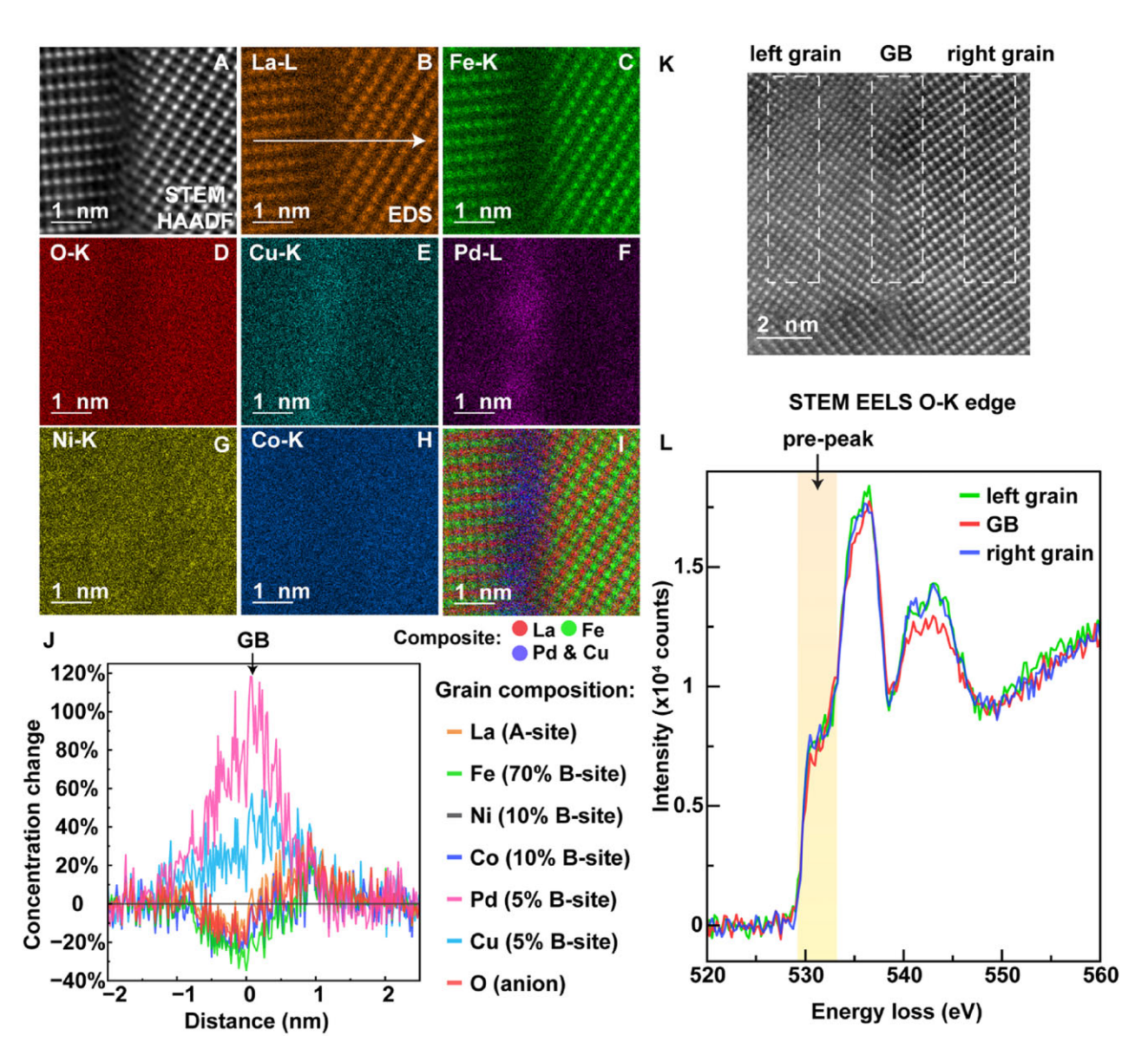


Fig. 1. Accumulation of V_O° at CCO GBs induces segregation of cations with high reducibility, such as of Pd and Cu, characterized by STEM EDS and EELS. (A-I) Atomic-resolution STEM EDS mapping of a CCO GB: (A) STEM high-angle annular dark-field (HAADF) survey image; (B) La-L with filter; (C) Fe-K with filter; (D) O-K; (E) Cu-K; (F) Pd-L; (G) Ni-K; (H) Co-K and (I) composite of La (red), Fe (green), mixed Cu and Pd (blue). (J) Concentration changes of each element across the GB shown in (A). The concentration profile is generated via extracting the profile of EDS signal along the direction perpendicular to the GB (marked as a white arrow in (BI)) and integral all the EDS signals, and then converting the EDS signal intensity to concentration with K-factor method. (K-L) STEM HAADF survey image of a GB in the CCO textured thin film (K), and corresponding EEL spectra of this GB (red), its left grain (green), and right grain (blue) (L), which are extracted from EELS mapping of the marked rectangle regions shown in (K). The EELS data were collected under dispersion of 0.25 eV/channel.

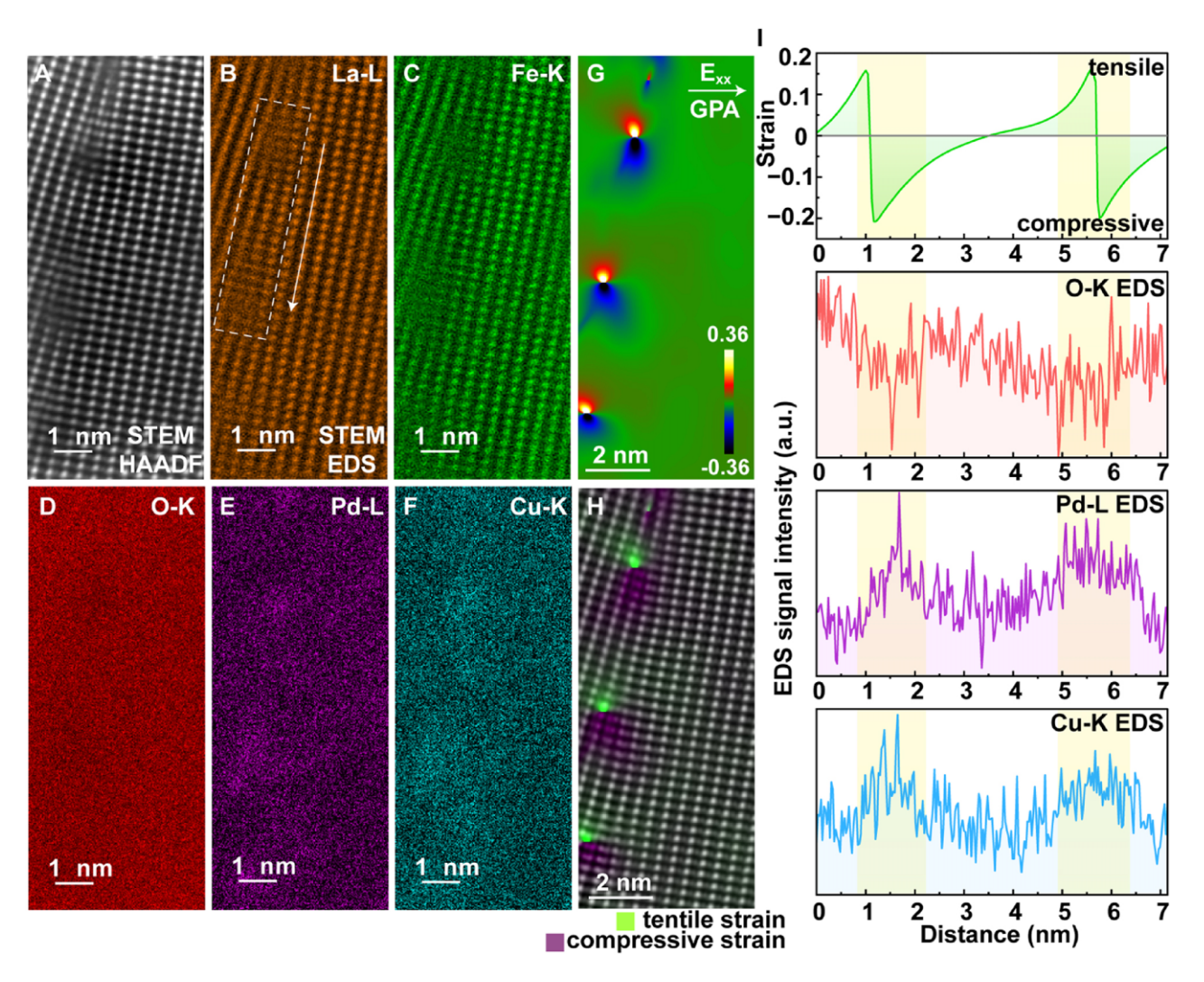


Fig. 2. Strong strain at dislocation cores induces localized oxygen deficiency and results in localized segregation of Cu and Pd. (A-F) STEM HAADF survey image of a low-angle tilt GB made up of a dislocation array (A), and corresponding STEM EDS mapping of filtered La-L (B), filtered Fe-K (C), O-K (D), Pd-L (E) and Cu-K (F). (G-H) Strain mapping around this GB along the marked E_{xx} direction via GPA (G), and composite image of the inverse fast Fourier transform (IFFT) image and GPA strain mapping along E_{xx} direction (H) to locate atomic arrangement causing the tensile strain (green) and compressive strain (purple) at this GB. (I) Profile of strain and EDS signal intensity along the GB dislocation array marked as an arrow in (B), integrated with data within the white rectangle (B). The regions with strong strain show severe deficiency of oxygen and rich EDS intensity of Pd and Cu, which are highlighted as yellow.

References

- 1. M. Brahlek et al., APL Materials 10 (2022), p. 110902. https://doi.org/10.1063/5.0122727
- 2. H. Guo et al., Matter 7 (2024), p. 1-16. https://doi.org/10.1016/j.matt.2023.12.012
- 3. X. Wang et al., Materials Research Letters 11 (2023), p. 196-204. https://doi.org/10.1080/21663831.2022.2135409
- 4. A.J. Wright and J. Luo, Journal of Materials Science 55 (2020), p. 9812-9827. https://doi.org/10.1007/s10853-020-04583-w
- 5. Y. Wang et al., Small Methods 7 (2023), p. 2201138. https://doi.org/10.1002/smtd.202201138
- 6. S.-T. Ko et al., Matter 6 (2023), p. 2395-2418. https://doi.org/10.1016/j.matt.2023.05.035
- 7. H. Vahidi et al., Advanced Functional Materials n/a (2024), p. 2315895. https://doi.org/10.1002/adfm.202315895
- 8. H. Guo et al., ChemRxiv. (2024). https://doi.org/10.26434/chemrxiv-2024-nbpfv
- 9. HG and WJB acknowledge NSF CAREER (DMR- 2042638) and ACS PRF (61961-DNI). HV, JL, and WJB were primarily supported by the National Science Foundation Materials Research Science and Engineering Center program through the UC Irvine Center for Complex and Active Materials (DMR-2011967). SS and KGA were primarily supported through the Center for Complex and Active Materials seed program. The authors acknowledge the use of facilities and instrumentation at the UC Irvine Materials Research Institute (IMRI), which is supported in part by the National Science Foundation through the UC Irvine Materials Research Science and Engineering Center (DMR-2011967).